Control of Vortex-Induced Oscillations in a Model Solid Rocket Motor: Flow Characterization and Secondary-Injection Experiments

10 July 2000

Prepared by

E. L. PETERSEN
Space Materials Laboratory
Laboratory Operations

J. W. MURDOCK
Vehicle Performance Subdivision
Vehicle Systems Division

Prepared for

SPACE AND MISSILE SYSTEMS CENTER
AIR FORCE MATERIEL COMMAND
2430 E. El Segundo Boulevard
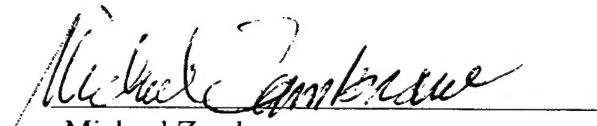Los Angeles Air Force Base, CA 90245

Engineering and Technology Group

THE AEROSPACE
CORPORATION
El Segundo, California

DTIC QUALITY INSPECTED 4

20001024 011

Michael Zambrana
SMC/AXE

REPORT DOCUMENTATION PAGE

Public reporting burden for this collection of information is estimated to average 1 hour per response, including the time for reviewing instructions, searching existing data sources, gathering and maintaining the data needed, and completing and reviewing the collection of information. Send comments regarding this burden estimate or any other aspect of this collection of information, including suggestions for reducing this burden to Washington Headquarters Services, Directorate for Information Operations and Reports, 1215 Jefferson Davis Highway, Suite 1204, Arlington, VA 22202-4302, and to the Office of Management and Budget, Paperwork Reduction Project (0704-0188), Washington, DC 20503.

1. AGENCY USE ONLY (*Leave blank*)	2. REPORT DATE 10 July 2000	3. REPORT TYPE AND DATES COVERED

4. TITLE AND SUBTITLE

Control of Vortex-Induced Oscillations in a Model Solid Rocket Motor: Flow Characterization and Secondary-Injection Experiments

5. FUNDING NUMBERS

F04701-93-C-0094

6. AUTHOR(S)

E. L. Petersen and J. W. Murdock

7. PERFORMING ORGANIZATION NAME(S) AND ADDRESS(ES)

The Aerospace Corporation
Laboratory Operations and Vehicle Systems Division
El Segundo, CA 90245-4691

8. PERFORMING ORGANIZATION REPORT NUMBER

TR-2000(8565)-15

9. SPONSORING/MONITORING AGENCY NAME(S) AND ADDRESS(ES)

Space and Missile Systems Center
Air Force Materiel Command
2430 E. El Segundo Boulevard
Los Angeles Air Force Base, CA 90245

10. SPONSORING/MONITORING AGENCY REPORT NUMBER

SMC-TR-00-29

11. SUPPLEMENTARY NOTES

12a. DISTRIBUTION/AVAILABILITY STATEMENT

Approved for public release; distribution unlimited

12b. DISTRIBUTION CODE

13. ABSTRACT (*Maximum 200 words*)

Vortex-driven instability in a solid rocket motor and its active control via secondary injection were studied in a cold-flow experimental model. All tests were conducted in an 86-cm-long, 5-cm-square airflow chamber. Twin orifice plates at the center of the chamber produced a 215-Hz vortex-driven pressure instability with 2% peak-to-peak oscillations near the first longitudinal chamber mode. Hot-wire anemometer data at the vortex shedding frequency indicate that the organized structures occur between the two orifice plates located at the center of the chamber and not between the orifice pair and the exit nozzle. Exploratory secondary-injection active control experiments were performed by pulsing a fast-acting solenoid valve at the upstream end of the chamber. The chamber pressure response (without orifice plates) to the pulsating secondary injection was characterized for various flow rates at frequencies of 100 and 150 Hz. Pressure perturbations of sufficient magnitude (1–5% peak-to-peak) to counter the vortex-driven instabilities were demonstrated. An active control scheme utilizing the present secondary-injection hardware will be the subject of future studies.

14. SUBJECT TERMS

Active control, Vortex, Combustion instability, Solid rocket motor, Secondary injection

15. NUMBER OF PAGES

20

16. PRICE CODE

17. SECURITY CLASSIFICATION OF REPORT UNCLASSIFIED	18. SECURITY CLASSIFICATION OF THIS PAGE UNCLASSIFIED	19. SECURITY CLASSIFICATION OF ABSTRACT UNCLASSIFIED	20. LIMITATION OF ABSTRACT

NSN 7540-01-280-5500

Acknowledgments

Contents

Figures

Tables

1. Introduction

A recurring problem in many solid rocket motors (SRMs) is the onset of internal pressure fluctuations that occur near the chamber's first longitudinal (1L) acoustic mode, potentially leading to thrust oscillations and vehicle vibrations. The source of this instability is a vortex-shedding mechanism wherein the frequency of the vortex shedding couples with the 1L mode.[1-5] The "locking in" of the vortex oscillation frequency with an acoustic mode requires feedback between the vortex formation point and some downstream impingement location, such as an internal flow obstruction and/or the exit nozzle.[1,5,6] Such vortex-shedding instabilities have been identified in many SRMs, including the Titan 34D,[4] the Space Shuttle SRB,[6] the Titan IV SRMU,[7] and the Ariane 5 P230.[8]

Figure 1 presents representative pressure- and frequency-time histories for a Titan IV SRMU static firing, taken from Dotson et al.[7] The organized pressure oscillations in Figure 1 occur between t = 57 and 63.5 s, when the shedding frequency coincides with the 1L acoustic mode near 1 Hz. A characteristic of vortex shedding in SRMs is the time-dependent oscillation frequency (Figure 1d) due to the changing internal flow geometry (and hence velocity) and the presence of an integer number of distinct vortices.[5,7] The tendency of the vortex shedding to lock in on an acoustic mode is robust; i.e., instability often occurs when the shedding/oscillation frequency is only within 25% of a natural mode frequency.[3-7] Although the vortex shedding in earlier motors comes from inhibitors placed between segments, the phenomenon can occur in more recent designs without inhibitors, such as the SRMU.[7]
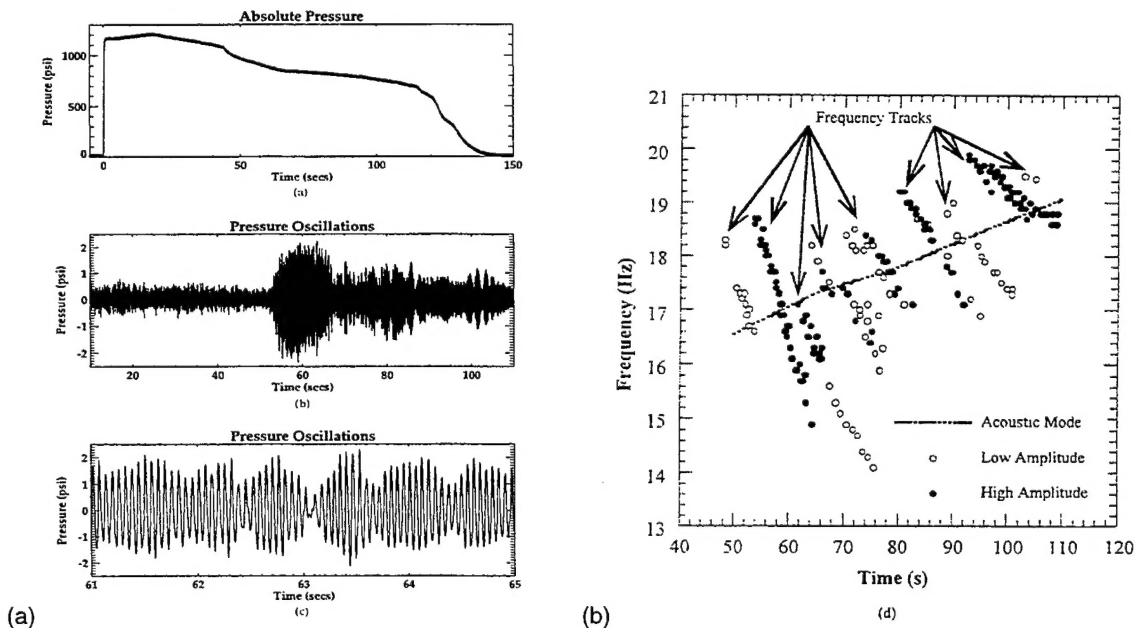

Figure 1.   Sample Titan IV SRMU pressure data showing the onset of vortex-driven instability near t = 57 s. (a) chamber pressure; (b) fluctuating component of chamber pressure; (c) snapshot during instability; (d) frequency time history of oscillations. Taken from Dotson et al.[7]

Over the past two years, The Aerospace Corporation has been studying the phenomenon of vortex-driven instability in SRMs with emphasis towards the development of an active control scheme to damp the resulting pressure oscillations.[9] Active control schemes provide an attractive alternative to passive damping techniques on vehicles where the vortex-shedding instability poses a significant problem. Currently a topic of active research, the control of combustion instability has been demonstrated using both closed- and open-loop schemes, employing techniques such as pulsed injection and acoustic excitation.[10] The goals of the present work, summarized in Table 1, include four primary phases: (I) background research; (II) demonstration of vortex-driven oscillations in a cold-flow model; (III) demonstration of active control at a fixed frequency; and (IV) demonstration of an adaptive, active control scheme.

The authors previously reported on Phases I and II, where the use of a cold-flow SRM model to produce fixed-frequency pressure oscillations at the 1L and 3L acoustic modes of the rig was confirmed.[9] Using a variable-area exit nozzle, the authors also demonstrated the production of real-time frequency tracks similar to those in Figure 1d. In the present report, the authors' earlier work is broadened to include detailed characterization of the flow apparatus and exploratory experiments of a secondary-injection-based active control scheme under Phase III (Table 1). A summary of the experimental apparatus is included first. Details of the rig's flow and acoustic characterization are given, and exploratory active control experiments involving secondary injection are described.

Table 1. Control of Vortex-Driven Instability Research Program.

Phase	Description	Goals
I	Background Research	Identify experiments and analysis pertaining to:
		1. vortex-driven instability
		2. active control of combustion instability
II	Demonstration of Instability	1. Design and fabricate cold-flow facility
		2. Demonstrate vortex-driven instability
		3. Demonstrate frequency tracks
		4. Characterize flow facility performance
III	Active Control Demonstration	1. Demonstrate secondary-injection technique
		2. Characterize chamber response
		3. Demonstrate open-loop instability suppression
		4. Perform closed-loop control of instability
IV	Adaptive Active Control	1. Optimize control scheme
		2. Design adaptive control scheme
		3. Demonstrate adaptive, active control of frequency tracks

2. Experimental Apparatus

Petersen and Murdock[9] describe the cold-flow model, facility, and diagnostics. An overview is provided herein. Differences in geometry and flow conditions between the present work and the earlier reference are highlighted.

2.1   Flow Chamber

Figure 2 presents a drawing of the experimental flow model, and Table 2 provides the major dimensions and flow parameters for the present experiments. The overall length, L, of the 5-cm-square Plexiglas duct is 86 cm. A fixed exit diameter of 1.91 cm was used. This exit orifice is smaller than the 2.54-cm exit used previously,[9] resulting in a lower chamber Mach number (and different instability frequency). Likewise, the variable-area exit reported previously was not employed in the present experiments since only a fixed oscillation frequency was needed for Phase III of the project (Table 1). Twin orifice plates located at the center of the chamber provide the vortex shedding and impingement; the orifice diameters, d, are 3.18 cm each, and the spacing, ℓ, is 3.2 cm. Located at the positions marked A-E are side- and bottom-wall instrumentation ports for pressure transducers and hot-wire anemometer probes.

Airflow through the Figure 2 SRM model is provided by pulling a vacuum with a large-capacity vacuum pumping system.[9] To model the conditions in a solid rocket engine, a constant primary entrance flow rate is set by a regulator valve upstream of the 20-hole array of choked orifices at x = 0 (Figure 2). The exit orifice at x = L is also choked, acoustically isolating the chamber. The total flow rate through the chamber at 65 torr was, nominally, 174 SLM (0.0035 kg/s) for the work herein, and the corresponding average chamber velocity and Mach number were 22.0 m/s and 0.064, respectively. These flow conditions resulted in an average chamber Reynolds number of 6×10^3.
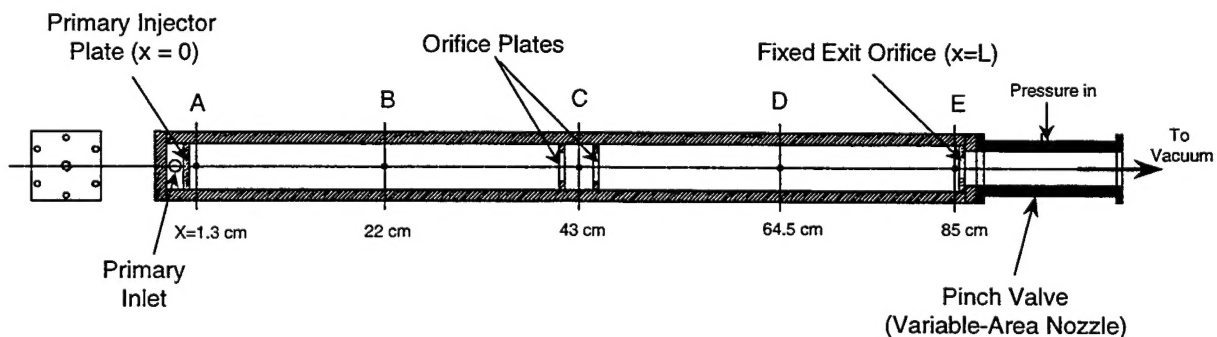

Figure 2.   Cold-flow model; material: Plexiglas. Twin orifice plates located at the center produce the vortex shedding and impingement mechanism. The variable-area nozzle was not employed in the present experiments. Instrumentation ports are located at positions A-E.

3

Table 2. Airflow Model Geometry and Flow Parameters.

Parameter	Value
Chamber Length (L)	85 cm
Chamber width (D)	5.08 cm
Exit Diameter	1.91 cm
Orifice Plate Diameter (d)	3.18 cm
Orifice Pair spacing (ℓ)	3.2 cm
Mach Number (M)	0.064
Average Velocity (U)	22.0 m/s
Flow Rate at 65 torr	0.0035 kg/s
	(174 SLM)

Two Endevco piezoresistive differential pressure transducers with a 70-kHz bandwidth, model 8510B-2, were used to monitor the chamber pressure at locations D and E (Figure 2). An Endevco miniature microphone with a 15-kHz bandwidth, model 8507C-2, was used to monitor the chamber acoustics at location E. The steady-state component of the chamber pressure was measured with an MKS Baratron transducer, model 122AA-00100AB, with digital readout model PDR-C-1B, also at position E. Hot-wire data were obtained using a two-channel, computer-based Streamware system from Dantec and a UEI WIN-30DS/4 data acquisition board. Various single-wire TSI and Dantec probes were employed.

A computer-based data acquisition system was utilized for signal acquisition. This system includes a National Instruments AT-MIO-16XE-10 card (16-channel, 100-kHz, 16-bit), a National Instruments BNC-2040 adapter board, and a 200-MHz GST Pentium computer with 32 MB of RAM. The typical data acquisition rate for the measurements herein was 5 kHz. The data acquisition routine was written using Labview software from National Instruments, version 4.1.

2.2   Secondary Injector

For the secondary injection experiments, a fast-response solenoid valve located at the front end of the chamber was employed, as shown in Figure 3. The valve is a Matrix 821 series, current-controlled solenoid valve, model OX821100C2XX. This valve has a maximum flow rate of 110 SLM and a combined opening and closing time of less than 2 ms, for a peak frequency of 500 Hz. A 24-V, 0.9-A input signal is required for maximum valve response.

An electrical circuit composed of a Fluke PM5136 function generator, a Hewlett Packard 6200B DC power supply, and a reed relay delivered the control signal to the pulsating solenoid valve. The power supply provided the current source, while the reed relay/function generator combination provided the oscillatory signal. The combined latching and opening time of the reed relay is less than 1 ms, and the function generator provided the square, 3-to-5-V TTL signal to the relay at the desired secondary-injection frequency.

4
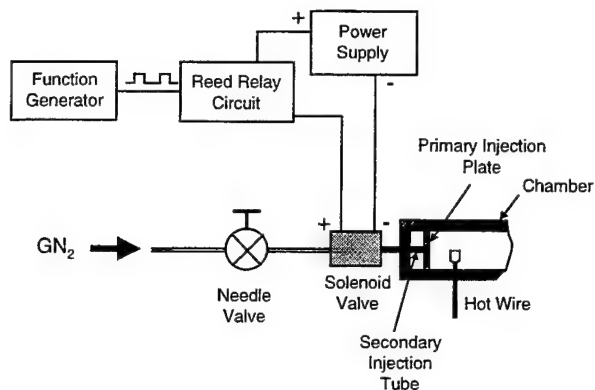
Figure 3. Secondary-injection apparatus and control scheme. The fast-response solenoid valve is a Matrix 821 series, capable of 500-Hz response and flows up to 110 SLM. The secondary fluid is N_2. A 1-ms reed-relay circuit switches the power to the solenoid at the function generator output frequency.

The solenoid valve mates to the chamber through an 8-cm-long, 3.2-mm tube (2.3-mm ID). A high-pressure supply of dry N_2 serves as the secondary-injection gas. Typically, the peak flow rate through the secondary-injection valve is between 30 and 90 SLM with a 7-bar supply pressure upstream of a manual regulator valve. Additional discussion of the secondary-injection system is provided in Section 4.

3. Flow Characterization

Further characterization of the flow model was performed in response to outstanding issues from earlier work.[9] Presented below are results from an acoustic characterization of the flow rig and some fundamental data pertaining to the vortex-shedding mechanism.

3.1   Chamber Acoustics

A standard acoustic-excitation technique was employed to identify the natural acoustic modes of the flow model. The setup included a signal source and an 8-Ω, 0.2-W loudspeaker positioned at the exit of the chamber. Two types of signals were sent to the speaker: (1) a sine wave at a set frequency using a Fluke PM5136 function generator, and (2) a white-noise signal provided by the data acquisition board and controlled via the National Instruments Virtual Bench waveform generator software. The acoustic response of the rig was monitored using pressure transducers at various locations within the chamber.

Sine-wave frequencies between 0 and 1000 Hz were sent to the loudspeaker; the chamber mode closest to the sine-wave frequency and its harmonics became excited when the speaker frequency was near the acoustic mode frequency. Figure 4a shows the response of the chamber to a 210-Hz sine wave. The Figure 4a results, taken with the microphone transducer at port E (Figure 2), are representative of any sine-wave frequency near a longitudinal chamber mode; i.e., each harmonic frequency is excited in addition to the speaker frequency. However, the strongest chamber response by far was always at the second longitudinal mode near 420 Hz, indicating that the flow model is most sensitive to this frequency. Similar results were obtained from white-noise excitation of the loudspeaker. Figure 4b shows a typical spectrum from the white noise excitation, with the 2L mode near 420 Hz dominating the acoustic response of the chamber.

Although the acoustic signatures in Figure 4 were obtained without the center orifice plates, similar results were obtained with the orifice plates present. Table 3 summarizes the predicted and measured acoustic modes of the SRM flow model, assuming a closed-closed (c-c) chamber between the front injection plane at x = 0 and the exit orifice plane at x = L (Figure 2) per

$$f_{cc} = \frac{nc}{2L},\tag{1}$$

where n is the acoustic mode integer, and c is the sound speed.

3.2   Vortex Shedding

In previous experiments,[9] the authors demonstrated fixed-frequency oscillations at 630 Hz, near the 3L c-c mode of the chamber (Table 3). However, to be within the 500-Hz limitations of the current
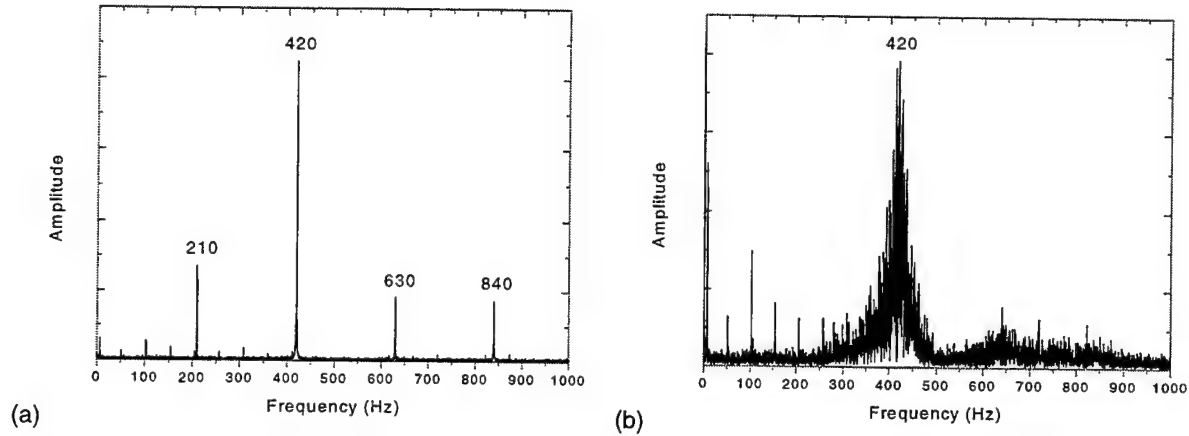
7

Figure 4. Acoustic response of the flow chamber to signals from a loudspeaker placed at the exit. The chamber is most sensitive to the 2L mode at 420 Hz. The microphone transducer was located near the exit (position E, Fig. 2). (a) Response to a 210-Hz sinusoidal excitation; this frequency triggered the maximum response, indicating coincidence with an axial mode. (b) Response to broad-band (white noise) excitation.

Table 3. Longitudinal Acoustic Frequencies of the Airflow Model in Hz (Accuracy: ±3 Hz).

Axial Mode	Measured	Calculated
1	210	202
2	420	405
2	630	607
3	840	808

secondary-injection hardware, vortex-driven oscillations near the first mode are more attractive. By keeping the spacing of the orifice pair constant at $\ell = 3.2$ cm, the oscillation frequency can be reduced by decreasing the chamber flow velocity per

$$f_{osc} \propto \frac{U}{\ell} m \qquad (2)$$

where U is the average chamber velocity, and m is the integer number of vortices.[7,9] This relationship between frequency and velocity was demonstrated by Petersen and Murdock[9] in real time by decreasing the exit area of the choked nozzle to obtain a time-varying oscillation frequency.

To accomplish this for a fixed oscillation frequency, the stationary exit-orifice diameter was changed from 2.54 cm to 1.91 cm. This decrease in exit area created a (nearly) factor-of-2 reduction in the average chamber Mach number (M) and velocity. The current values are listed in Table 2. The net effect was to change the oscillation frequency to a value near the 1st acoustic mode. Figure 5a shows
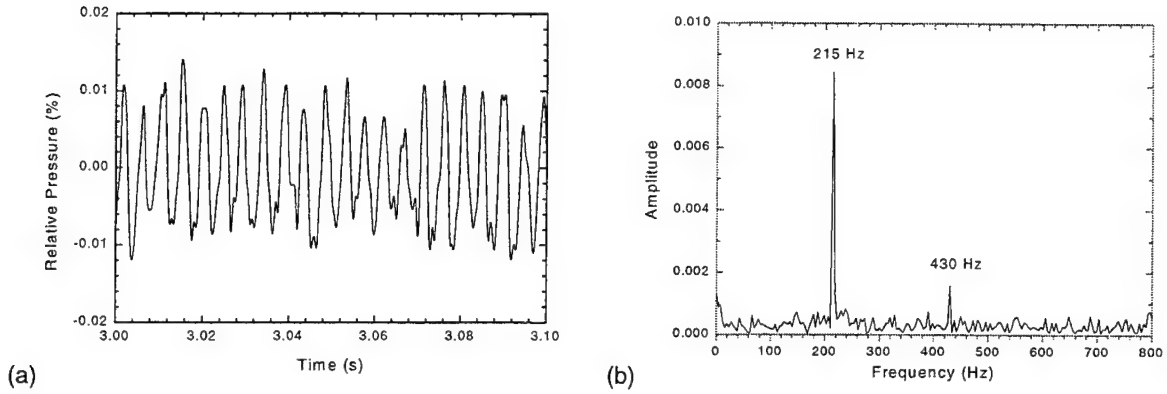
8

Figure 5.   Pressure measurements of the vortex-induced instability for the current configuration
(Table 2). (a) Snapshot of pressure signal. (b) Pressure amplitude spectrum.

the oscillatory component of the chamber pressure, and Figure 5b shows the spectral content of the organized oscillations. The peak-to-peak (p-p) response of the pressure is approximately 2% of the mean pressure at an instability frequency of 215 Hz. A harmonic of the 215-Hz vortex-driven perturbation appears at 430 Hz. However, as discussed below, the 430-Hz portion of the instability is not due to a vortex-shedding frequency but, rather, to the fact that the chamber is extremely sensitive to the 2nd longitudinal mode near 420 Hz (Figure 4). Consequently, any harmonic of this 420-Hz frequency (e.g., the 215 Hz instability in the present case) would be expected to acoustically excite the 2L chamber mode.

The vortex-shedding characteristics were further explored by placing a hot-wire probe into the flow field. As demonstrated by Dunlap and coworkers,[3,4] a hot-wire anemometer can sense the vortex-shedding frequency when placed in the region where the organized structures exist. Figure 6 displays the hot-wire anemometer results when the probe is placed at location C, between the two orifice plates (Figure 2). The raw hot-wire signal in Figure 6a indicates the presence of organized structures, and the fast Fourier transform in Figure 6b leads to the conclusion that vortices are indeed being formed and propagated at the same frequency as the ordered chamber pressure oscillations, 215 Hz (Figure 5). The 430-Hz frequency seen in Figure 5 does not show up in the Figure 6 anemometer trace, indicating that it is predominantly an acoustic tone and not a shedding frequency.
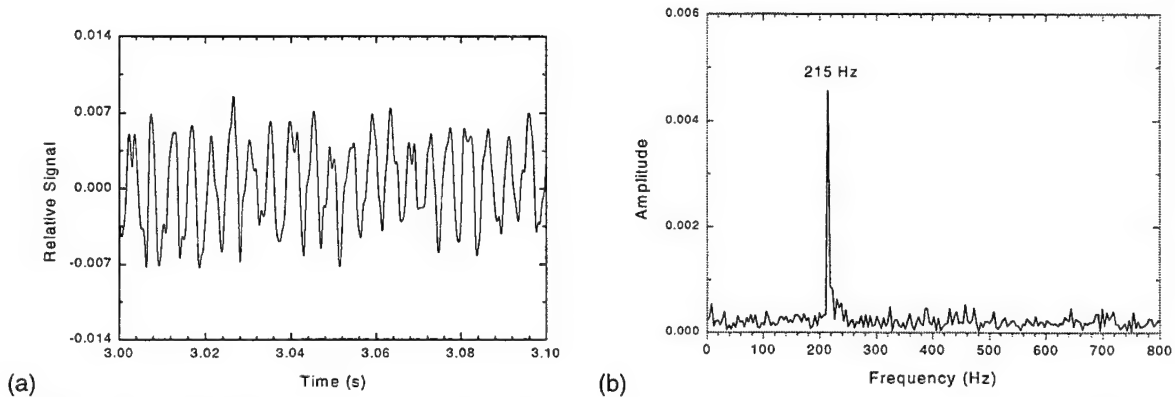

Figure 6.   Hot-wire measurement with the probe located between the two orifice plates (position C,
Fig. 2). (a) Snapshot of raw hot-wire signal. (b) Amplitude spectrum of hot-wire trace.

9

From the data in Figure 6, one can conclude that organized structures at the instability frequency exist between the two central orifice plates. However, it has been postulated that the formation and impingement points in an actual SRM do not have to be from baffle to baffle, but can instead be between a baffle and the nozzle exit.[6,7] To investigate the presence of coherent structures between the orifice pair and the nozzle in the present simulation, a hot-wire was placed at location D, midway between the pair and the exit plane (Figure 2).

Figure 7 presents a typical hot-wire measurement at location D. The raw trace in Figure 7a shows a high turbulence level, but the spectral content (Figure 7b) shows no distinct frequency. The Figure 7b frequency spectrum implies that no organized vortices exist downstream of the last orifice plate in the present experiment. Therefore, the orifice pair serves as the vortex formation and impingement points required for the instability mechanism.

However, this result is not surprising because the present cold-flow simulation has only an axial flow component, as opposed to actual SRMs, which include inherent vorticity due to radial flow from the solid propellant walls.[11] The inherent lack of vorticity in the present rig implies that organized structures have a relatively short lifetime therein. Hence, it is more likely for organized vortices to exist only between the closely spaced orifice plates in the present experiment ($\ell = 3$ step heights) because such structures would be unlikely to remain coherent as far downstream as the nozzle exit plane (40 step heights from the formation point).

For similar reasons, the Figure 7 result does not imply that organized structures do not exist between an interior formation point and the nozzle in an actual SRM; it merely proves the lack of coherent vortices between the orifice plates and the exit nozzle in the present cold-flow simulation. Antoine et al.[12,13] have shown that radial flow in a cold-flow model leads to distinct structures that last considerably longer than those in an axial-flow model.
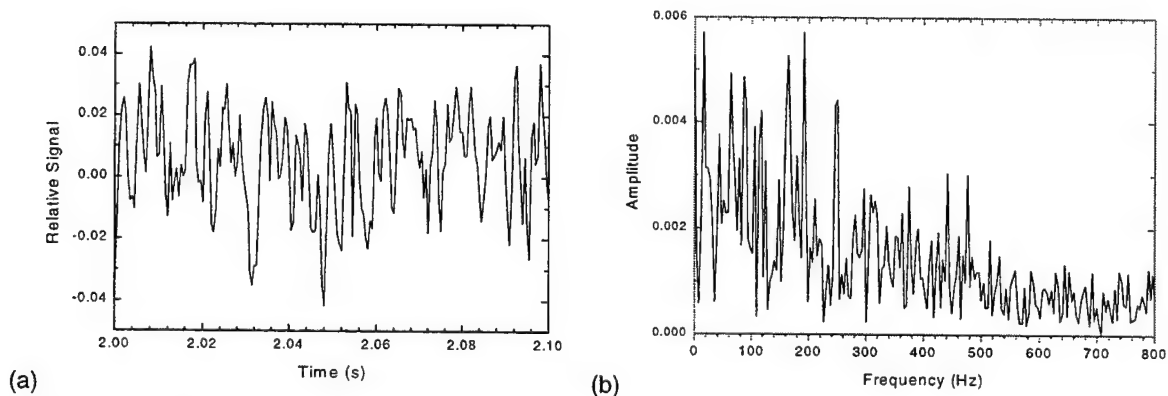

Figure 7. Hot-wire measurement with the probe located halfway between the orifice pair and the exit nozzle (position D, Fig. 2). (a) Snapshot of raw hot-wire signal. (b) Amplitude spectrum of hot-wire trace.

4. Secondary-Injection Experiments

Phase III of the research program involves the demonstration of an active control scheme for the suppression of vortex-driven oscillations in a solid rocket engine. The oscillatory injection of a secondary fluid is the chosen control technique. Secondary injection of both liquid and gaseous propellants has been used by other researchers to suppress instabilities in combustion applications.[10,14-19] By controlling the frequency, phasing, and magnitude of the secondary fluid, the combustion oscillations can be countered and suppressed.

In the present cold-flow demonstration, the advantages of energy release from the secondary propellant are not available. Hence, secondary-injection-based instability suppression in cold flows must come only from mass addition to the chamber. From the theoretical calculations presented previously,[9] the authors estimated that the suppression of a 1% p-p pressure oscillation at 200 Hz would require a peak secondary-injection mass flow rate that is approximately 25% of the primary mass flow rate. The secondary injection scheme shown in Figure 3 was designed accordingly.

Exploratory secondary-injection experiments were performed at two injection frequencies: 100 and 150 Hz. For these tests, the twin orifice plates were removed so that no pressure perturbation existed, ensuring that the pressure response measured was due only to the secondary injection. To isolate the injector performance, the initial experiments were performed without the primary airflow. Later experiments included both the primary and secondary flows (see below).

Figure 8 presents typical results for a 100-Hz injection frequency. A hot wire placed at the exit of the injector (Figure 3) was used to infer the time history of the injector output. The hot-wire data are shown in Figure 8a in comparison with the TTL signal used to open and close the fast-response solenoid valve. A 100-Hz oscillatory pattern is evident in the injector exit flow, but apparent limitations in the valve response and/or control system lead to an asymmetric injection time history. The corresponding 100-Hz input signal is intentionally asymmetric to help compensate for the nonideal valve response. The pressure trace in Figure 8b displays an organized oscillation, as expected from the
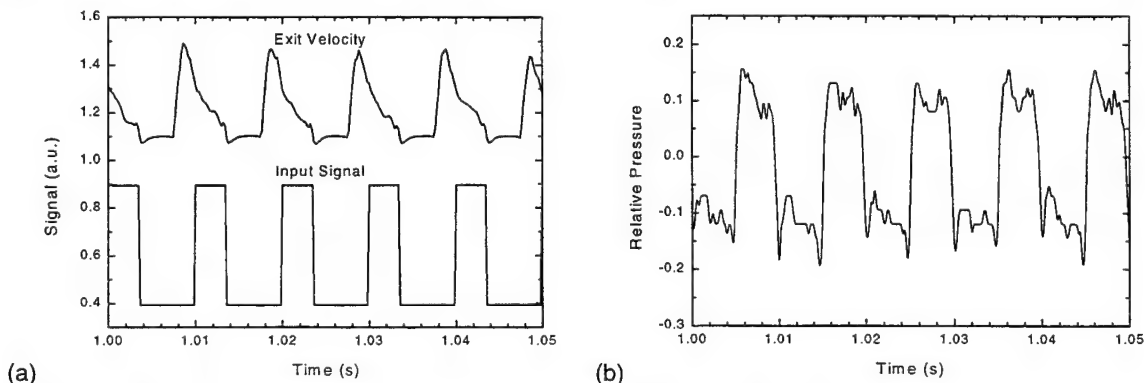

Figure 8. Secondary injection at 100 Hz with no primary flow. (a) Secondary-injection input signal and exit velocity. (b) Chamber pressure response

11

oscillatory mass flow addition to the chamber. Similar results are displayed in Figure 9 for a 150-Hz injection frequency. For the chamber pressure traces in Figures 8 and 9, the transducer was located at position E, immediately upstream of the exit nozzle.

The major frequencies of the chamber pressure oscillations are presented in Figure 10a for the 100-Hz frequency and Figure 10b for the 150-Hz frequency. In both spectra, the dominant frequency is the primary driving frequency of the valve. However, because of the nonideal injector response, harmonics of the driving frequency show up in the chamber pressure. These additional frequencies, although small in amplitude, are undesirable for the final control scheme. Additional measures are underway to remedy the situation.

Nonetheless, a significant conclusion of these exploratory secondary-injection experiments is the fact that the desired chamber-response characteristics are produced. That is, the secondary-injection technique must be able to perturb the chamber in the same manner as the vortex-driven instability in order to counteract and suppress the instability. Figure 11 shows a typical chamber pressure response to secondary injection at 150 Hz when the primary gas is flowing. The resulting peak-to-

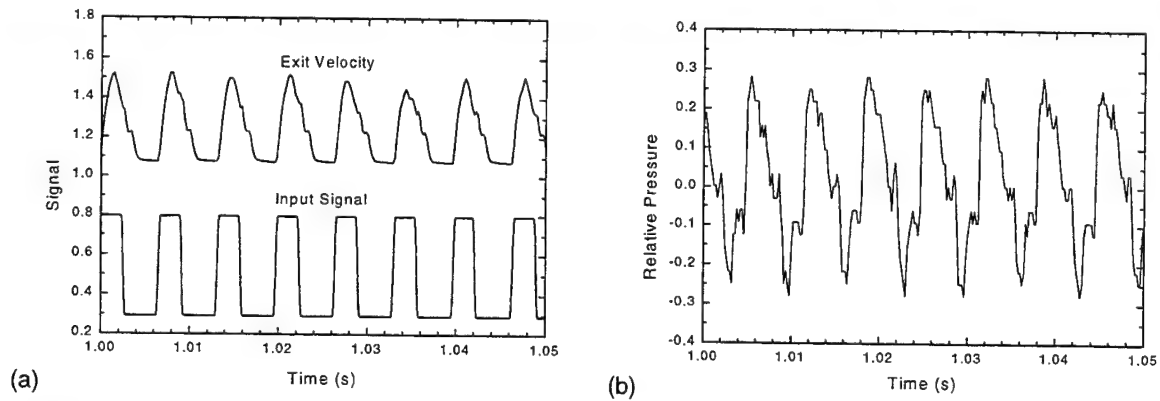Figure 9.   Secondary injection at 150 Hz with no primary flow. (a) Secondary-injection input signal and exit velocity. (b) Chamber pressure response.
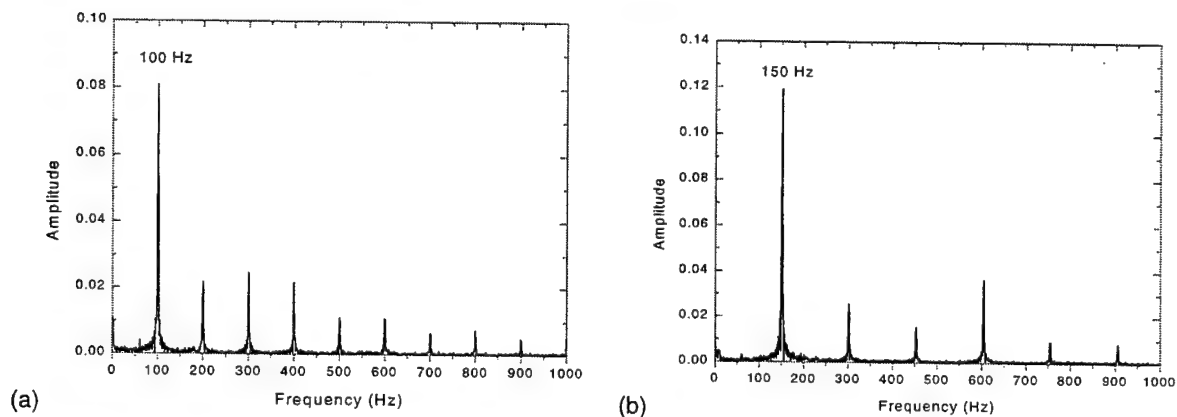

Figure 10.   Chamber pressure spectral response to secondary injection. (a) Pressure amplitude spectrum for 100-Hz injection frequency. (b) Pressure amplitude spectrum for 150-Hz injection frequency. The pressure traces are presented in Figs. 8 and 9.

12
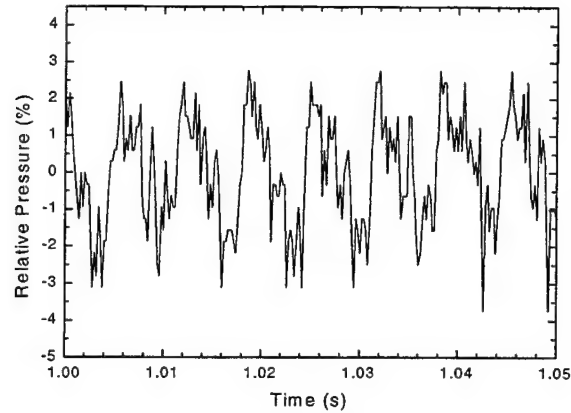
Figure 11. Chamber pressure oscillations with the primary flow on and a 150-Hz secondary-injection frequency; P = 68 torr, ε = 0.47. The p-p oscillations are nearly 5% of the total chamber pressure.

peak pressure oscillations for the Figure 11 case (initial chamber pressure of 65 torr) are nearly 5% of the chamber pressure in magnitude. This effect is more than adequate when compared with the magnitude of the vortex-induced oscillations, which are typically less than 5% in the present flow rig. The magnitude of the chamber oscillations due to secondary injection can be controlled by increasing or decreasing the injector mass flow rate accordingly.[9]

5. Active Control Experiments

Given the above demonstration of the secondary-injection scheme, the next step in the experimental program is the use of the scheme to suppress the vortex-driven pressure oscillations. For these experiments, the twin orifice plates will be placed back into the chamber to produce the 215-Hz instability seen in Figure 5. By pulsing the secondary injector (i.e., the Figure 3 solenoid valve) at the same 215-Hz frequency, pressure perturbations of a magnitude similar to the instability fluctuations will be introduced into the chamber. With proper phasing, the two pressure fluctuations should cancel, leading to a reduction in the magnitude of the ordered oscillations.

To accomplish the required phasing, the Figure 3 secondary-injection scheme can be extended to the proposed closed-loop control scheme in Figure 12. A pressure transducer located in the chamber provides the feedback signal for the closed-loop control. This transducer signal is sent through a filter/amplifier (SRS Model SR560) where it is ac-filtered to isolate the oscillatory component. The processed pressure signal then becomes the reference input signal to a lock-in amplifier (SRS Model SR830 DSP). An internally generated sine wave of known phase relative to the reference signal is sent from the lock-in amplifier to a pulse generator, where it serves as the TTL trigger for a pulse generator (BNC Model 500). The resulting signal from the pulse generator provides the input TTL signal for the secondary-injector control circuit, thus closing the loop with the SRM model.

Initial active control experiments using the Figure 12 scheme will explore the optimum phase relationship between the chamber oscillations and the secondary injector. The optimum phase will be the one that results in maximum suppression of the pressure fluctuations. Additional control variables such as the secondary flow rate, pulse shape, etc. will be explored separately as needed. Once
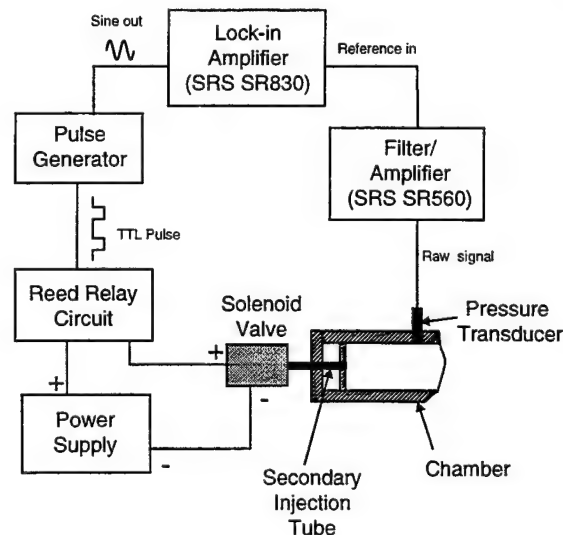
Figure 12. Schematic diagram of the proposed closed-loop active control scheme using the Fig. 3 secondary injector.

15

an active control scheme is demonstrated, Phase III of the current project will be satisfied (Table 1). Further optimization of the control scheme will be performed under Phase IV, which includes the development of an adaptive control scheme to suppress instabilities with a time-dependent magnitude and oscillation frequency.

6. Summary

Flow characterization and secondary injection experiments were performed on a model solid rocket motor. The airflow experiments were part of an on-going research program with the goal of demonstrating a secondary-injection-based active control scheme for the suppression of vortex-driven instabilities. An orifice pair located at the center of the 86-cm-long flow model provides the vortex shedding and impingement mechanism. The acoustic modes of the chamber were determined using a loudspeaker and microphone transducer; the longitudinal modes agree well with those predicted for a closed-closed chamber. Vortex-driven pressures (2% p-p) near the first longitudinal mode were demonstrated at a 215-Hz frequency. Hot-wire measurements of the vortex-shedding phenomenon lead to the conclusion that organized structures at the oscillation frequency exist between the twin orifice plates and not between the orifice pair and the exit nozzle.

The front-end secondary-injection scheme consists of a fast-acting solenoid valve capable of frequencies up to 500 Hz. Exploratory experiments were conducted with the vortex-generating orifice plates removed from the flow field. The chamber response to secondary-injection frequencies of 100 and 150 Hz was characterized with and without a primary airflow. Chamber pressure oscillations of sufficient magnitude (as high as 5% p-p) to suppress the instabilities were demonstrated. A closed-loop active control scheme employing the current secondary-injection hardware was detailed, the future results of which will be presented in a later report.

References

1. Flandro, G. A. and Jacobs, H. R., "Vortex-Generated Sound in Cavities," in *Aeroacoustics: Jet and Combustion Noise; Duct Acoustics, Progress in Aeronautics and Astronautics*, Vol. 37, Nagamatsu (Ed.), AIAA, 1975, pp. 521–533.

2. Culick, F. E. C. and Magiawala, K., "Excitation of Acoustic Modes in a Chamber by Vortex Shedding," *Journal of Sound and Vibration*, Vol. 64, No. 3, 1979, pp. 455–457.

3. Dunlap, R. and Brown, R. S., "Exploratory Experiments on Acoustic Oscillations Driven by Periodic Vortex Shedding," *AIAA Journal*, Vol. 19, No. 3, 1981, pp. 408–409.

4. Brown, R. S., Dunlap, R., Young, S. W., and Waugh, R. C., "Vortex Shedding as a Source of Acoustic Energy in Segmented Solid Rockets," *Journal of Spacecraft and Rockets*, Vol. 18, No. 4, 1981, pp. 312–319.

5. Nomoto, H. and Culick, F. E. C., "An Experimental Investigation of Pure Tone Generation by Vortex Shedding in a Duct," *Journal of Sound and Vibration*, Vol. 84, No. 2, 1982, pp. 247–252.

6. Flatau, A. and VanMoorhem, W., "Prediction of Vortex Shedding Responses in Segmented Solid Rocket Motors," AIAA paper 90-2073, July 1990.

7. Dotson, K. W., Koshigoe, S., and Pace, K. K., "Vortex Shedding in a Large Solid Rocket Motor Without Inhibitors at the Segment Interfaces," *Journal of Propulsion and Power*, Vol. 13, No. 2, 1997, pp. 197–206.

8. Kourta, A., "Vortex Shedding in Segmented Solid Rocket Motors," *Journal of Propulsion and Power*, Vol. 12, No. 2, 1996, pp. 371–376.

9. Petersen, E. L. and Murdock, J. W., "Active Control of Vortex-Driven Oscillations in a Solid Rocket Motor Using a Cold-Flow Simulation," AIAA Paper 99-0860, Jan. 1999. Also, ATR-99(8426)-1.

10. McManus, K. R., Poinsot, T., and Candel, S. M., "Review of Active Control of Combustion Instabilities," *Progress in Energy and Combustion Science*, Vol. 19, 1993, pp. 1–29.

11. Culick, F. E., "Rotational Axisymmetric Mean Flow and Damping of Acoustic Waves in a Solid Propellant Rocket," *AIAA Journal*, Vol. 4, No. 8, 1966, pp. 1462–1464.

12. Anthoine, J., Planquart, P., and Olivari, D., "Cold Flow Investigation of the Flow Acoustic Coupling in Solid Propellant Boosters," AIAA Paper 98-0475, Jan. 1998.

13. Anthoine, J., Olivari, D., Hulshoff, S., and Van Rooij, M., "Qualitative Model of Vortex Induced Oscillations in a Model of Solid Propellant Boosters," AIAA Paper 98-2270, July 1998.

14. Neumeier, Y. and Zinn, B. T., "Experimental Demonstration of Active Control of Combustion Instabilities Using Real-Time Modes Observation and Secondary Fuel Injection," *Twenty-Sixth Symposium (International) on Combustion*, The Combustion Institute, Pittsburgh, 1996, pp. 2811–2818.

15. Neumeier, Y., Peled, A., Liu, Y., and Zinn, B. T., "Theoretical and Experimental Investigation of the Performance of an Actively Controlled Fuel Actuator," AIAA Paper 98-0355, Jan. 1998.

16. Yu, K. H., Parr, T. P., Wilson, K. J., Schadow, K. C., and Gutmark, E. J., "Active Control of Liquid-Fueled Combustion Using Periodic Vortex-Droplet Interaction," *Twenty-Sixth Symposium (International) on Combustion*, The Combustion Institute, Pittsburgh, 1996, pp. 2843–2850.

17. Yu, K., Wilson, K. J., and Schadow, K. C., "Active Instability Suppression by Controlled Injection of Liquid Fuel," AIAA Paper 97-3324, July 1997.

18. Yu, K., Wilson, K. J., and Schadow, K. C., "Liquid-Fueled Combustion Control: Scale-Up Experiments and Effect of Fuel Droplet Size," AIAA Paper 99-0328, Jan. 1999.

19. Chang, E. and Kailasanath, K., "Active Control of Combustion Instabilities Using Timed Injection of High Energy Fuels," AIAA Paper No. 98-3765, July 1998.

LABORATORY OPERATIONS

The Aerospace Corporation functions as an "architect-engineer" for national security programs, specializing in advanced military space systems. The Corporation's Laboratory Operations supports the effective and timely development and operation of national security systems through scientific research and the application of advanced technology. Vital to the success of the Corporation is the technical staff's wide-ranging expertise and its ability to stay abreast of new technological developments and program support issues associated with rapidly evolving space systems. Contributing capabilities are provided by these individual organizations:

Electronics and Photonics Laboratory: Microelectronics, VLSI reliability, failure analysis, solid-state device physics, compound semiconductors, radiation effects, infrared and CCD detector devices, data storage and display technologies; lasers and electro-optics, solid state laser design, micro-optics, optical communications, and fiber optic sensors; atomic frequency standards, applied laser spectroscopy, laser chemistry, atmospheric propagation and beam control, LIDAR/LADAR remote sensing; solar cell and array testing and evaluation, battery electrochemistry, battery testing and evaluation.

Space Materials Laboratory: Evaluation and characterizations of new materials and processing techniques: metals, alloys, ceramics, polymers, thin films, and composites; development of advanced deposition processes; nondestructive evaluation, component failure analysis and reliability; structural mechanics, fracture mechanics, and stress corrosion; analysis and evaluation of materials at cryogenic and elevated temperatures; launch vehicle fluid mechanics, heat transfer and flight dynamics; aerothermodynamics; chemical and electric propulsion; environmental chemistry; combustion processes; space environment effects on materials, hardening and vulnerability assessment; contamination, thermal and structural control; lubrication and surface phenomena.

Space Science Application Laboratory: Magnetospheric, auroral and cosmic ray physics, wave-particle interactions, magnetospheric plasma waves; atmospheric and ionospheric physics, density and composition of the upper atmosphere, remote sensing using atmospheric radiation; solar physics, infrared astronomy, infrared signature analysis; infrared surveillance, imaging, remote sensing, and hyperspectral imaging; effects of solar activity, magnetic storms and nuclear explosions on the Earth's atmosphere, ionosphere and magnetosphere; effects of electromagnetic and particulate radiations on space systems; space instrumentation, design fabrication and test; environmental chemistry, trace detection; atmospheric chemical reactions, atmospheric optics, light scattering, state-specific chemical reactions and radiative signatures of missile plumes.

Center for Microtechnology: Microelectromechanical systems (MEMS) for space applications; assessment of microtechnology space applications; laser micromachining; laser-surface physical and chemical interactions; micropropulsion; micro- and nanosatellite mission analysis; intelligent microinstruments for monitoring space and launch system environments.

Office of Spectral Applications: Multispectral and hyperspectral sensor development; data analysis and algorithm development; applications of multispectral and hyperspectral imagery to defense, civil space, commercial, and environmental missions.